Climatology and trends of the middle atmospheric temperature (33–87 km) as seen by Rayleigh lidar over the south of France

Alain Hauchecorne, Marie-Lise Chanin, Philippe Keckhut

JOURNAL OF GEOPHYSICAL RESEARCH, VOL. 96, NO. D8, PAGES 15,297–15,309, AUGUST 20, 1991

CLIMATOLOGY AND TRENDS OF THE MIDDLE ATMOSPHERIC TEMPERATURE (33-87 KM) AS SEEN BY RAYLEIGH LIDAR OVER THE SOUTH OF FRANCE

Alain Hauchecorne, Marie-Lise Chanin, and P. Keckhut

Service d'Aéronomie du Centre National de la Recherche Scientifique,

Verrières le Buisson, Cedex, France

Abstract. The technique of the Rayleigh lidar provides temperature profiles with a good temporal and vertical resolution in the middle atmosphere. Data obtained by 2 Rayleigh lidars set up at the Observatory of Haute-Provence (44°N, 6°E) and at Biscarrosse (44°N, 1°W) from 1978 to 1989 led to a unique set of data of 1200 night-mean temperature profiles from 37 to 87 km. A climatology of the temperature over the south of France has been established from this data base and new results concerning both the short-term and long-term variability of the middle atmosphere are presented in this paper.The observed temperature around 44°N, 0°W is in general colder than the mean temperature given in the COSPAR International Reference Atmosphere (1986) near 75 km and warmer above 80 km. A clear semi-annual variation is observed near 65 km with maxima occurring just after the equinoxes. The study of the short-term variability indicates clearly two frequency domains: long periods below 65 km with a maximum in December-January which relate to planetary waves and shorter periods above 65 km induced by the breaking of gravity waves. A correlation with the 11-year solar cycle, negative in the stratosphere and positive in the mesosphere, is found to be well above the 95% confidence level with an amplitude larger in winter than in summer. However, with only 11 years of data it is obviously difficult to conclude that this atmospheric perturbation is induced by the solar forcing. A cooling of the mesosphere of about -4 K/decade at 60-70 km is found but is at the limit of the 95% confidence level, whereas we do not observe any significant trend in the stratosphere.

Introduction

The climatology of the structure of the middle atmosphere above 30 km has been studied first from in situ rocket measurements since the 1950s and then by remote sensing satellite experiments. The rocketsondes provide good vertical profiles up to 60 km but present some problems of accuracy beyond 60 km due to the rarefaction of the atmosphere and the very high speed of the sonde. Furthermore, the profile is instantaneous and affected by the short-term gravity waves. The number of soundings is limited by the cost of the launch and the equipment. Falling spheres are used to obtain temperature derived from density measurements up to 90 km [Schmidlin, 1981] but not on a regular basis. Satellite experiments alone are able to give a global coverage of the temperature field but have a relatively low horizontal and vertical resolution. The mesospheric temperature has been measured by infrared limb sounders from 1975 to 1982: Pressure Modulated Radiometer (PMR; Curtis et al. [1974]), Selective Chopper Radiometer [Ellis et al., 1973], Limb Infrared Mesospheric Sounder [Gille et al., 1984] and Stratosphere and Mesosphere Sounder [Drummond et al., 1980]. The upper stratosphere is covered continuously by the Stratospheric Sounding Unit instruments (SSU; Miller et al. [1980]) on board the NOAA operational satellites, but with a very poor vertical resolution. The climatology of the middle atmospheric temperature has been obtained by Barnett and Corney [1985] from PMR data over the 1975-1978 period and is the base of the new COSPAR International Reference Atmosphere (CIRA 1986; Barnett and Corney, [1985]). It gives the best available representation of the latitudinal, longitudinal and seasonal variations of the temperature, at least up to 65 km. However, the short-term and interannual variability of the atmosphere is not taken into account in the CIRA 1986. This climatology has been completed in the mesosphere by Clancy and Rusch [1989] from global observations of UV limb radiances from the Solar Mesosphere Explorer (SME) for the period 1982-1986. Mesospheric temperature will not be measured from space until the launch of the Upper Atmosphere Research Satellite at the end of 1991.

The technique of Rayleigh lidar has been shown capable of obtaining temperature profiles with a good vertical resolution from 30 to 90 km and to follow the temporal evolution of this parameter at all time scales from fractions of an hour to years [Hauchecorne and Chanin, 1980; Chanin and Hauchecorne, 1984]. Two Rayleigh lidars, located in the south of France, are operated about 100 nights per year since 1981 at the Observatory of Haute-Provence (44°N, 6° E) and since 1986 at Biscarrosse (44°N, 1° W). The climatology obtained from more than 1000 nightly average profiles will be presented and compared with previous studies. We will emphasize the importance of temperature variance associated with different phenomena, planetary wave propagation, breaking of gravity waves, quasi-biennial oscillation (QBO) and the 11-year solar cycle.

Lidar description

Data used in this study have been obtained with the Rayleigh lidar technique, which is based on the backscattering of a pulsed laser beam by atmospheric molecules. The temporal analysis of the echo provides the vertical profile of atmospheric density in relative value. The temperature profile is deduced from the density profile using classical hypothesis, hydrostatic equilibrium and perfect gas law, and is obtained in absolute value. The method is described in detail in previous publications [Hauchecorne and Chanin, 1980; Chanin and Hauchecorne, 1984] and only indications relevant to this study will be given here.

The experimental data set has been obtained from October 1978 to December 1989 with two lidar stations based in the south of France: Observatory of Haute-Provence (OHP, 44°N, 6°E) and Biscarrosse (BIS, 44°N, 1°W). The main characteristics of the two lidars are presented in Table 1.

The quality of the data at OHP has been improved in December 1983 by using a more powerful data acquisition system. The BIS lidar may be operated during daytime by using a smaller field of view (0.1 mrad) and a Fabry-Perot interferometer to reduce the background light. However, temperature profiles are limited to 60 km in this mode and will not be used in the climatological study.

Paper number 91JD01213.
0148-0227/91/91JD-01213$05.00

Table 1. Lidar characteristics

	OHP	BIS
	Emission	
Laser	Nd-YAG	Nd-YAG
Wavelength	532 nm	532 nm
Repetition rate	15 Hz	30 Hz
Energy per shot	400 mJ	200 mJ
Divergence	1.10^{-4} rad	1.10^{-4} rad
	Reception	
Telescope diameter	80 cm	120 cm
Field of view	2.10^{-4} rad	2.10^{-4} rad
Distance emission-reception	60 cm	coaxial
Vertical resolution	300 m	300 m
Detection mode	photon counting	photon counting
Spectral bandwidth	1 nm	1 nm (day 20 pm)
	Operation mode	
Period of operation	October 1978 --->	March 1986 --->
Low altitude channel	April 1987 --->	April 1986 --->
Semi-automatic mode	no	September 1988 --->
Daytime measurement	no	yes

Discussion of the method

The Role of Mie Scattering

The Rayleigh lidar method assumes that the scattering light is only due to Rayleigh scattering by molecules and that the Mie scattering due to aerosols is negligible. Due to the presence of the stratospheric aerosols layer around 20 km, it is not possible to use measurements below 30 km. Multi-wavelength measurements have shown that outside the periods following major volcanic eruptions the Mie scattering contribution may be neglected above 30 km. However, after the El Chichon eruption in May 1982 aerosols have been detected as high as 38 km [Lefrère et al., 1981] and data contaminated by aerosols have been suppressed in 1982 and 1983 for the data base used in this paper.

Hydrostatic and Constant Mixing Ratio Hypothesis

The determination of the temperature from the density profile is based on the assumption that the atmosphere is in hydrostatic equilibrium. This is not true locally in strong turbulent layers; however, taking into account the time and spatial integration of the lidar measurement, such an hypothesis is verified with a good level of accuracy. It is also assumed that the major gases of the atmosphere are in constant mixing ratio, which is true up to the homopause near 100 km. Above this level the mean molecular weight of the atmosphere slowly decreases with height.

Optic and Electronic Effects

The determination of the temperature assumes that the measured scattering is proportional to the atmospheric density divided by the square of the distance, with a constant of proportionality independent of the altitude. This constant may be affected by two types of problems:

Focalization and parallax effects. The scattered light is collected at the focus of the reception telescope but this focus depends on the altitude of the scattered light. In addition, if the emission and the reception telescopes are not coaxial, an effect of parallax depending on the altitude is observed. In order to minimize these effects it is necessary to reduce the divergence of the laser beam, to minimize the distance between the emission and the reception, to have a telescope field of view large enough to include all these effects and to rely on a very good procedure to check the parallelism between the two telescope axis.

Dynamic of the signal. Two of the problems of the Rayleigh lidar are the large dynamic of the signal which varies by a factor of 10^5 from 30 to 90 km and the very high illumination of the detector due to the diffusion of the laser light by the lower atmosphere. These difficulties are resolved by using a mechanical or an electronic shutter to protect the detector from the lower atmosphere diffusion and by adding a second detector, which receives a few percents of the signal, for the lower part of the profile.

Accuracy

Errors affecting these measurements may be divided into two parts:

1. The statistical error due to the photon counting is easy to evaluate. This error is reduced when the temporal and spatial resolution are degraded. For long-term trends and planetary wave studies, average nighttime profiles are used, integrated during 3 to 4 hours and with a 3 km vertical resolution. In this case, the typical values of the statistical error are

from 30 to 70 km	< 0.3 % in density	<1K in temperature
at 80 km	1 % in density	3 K in temperature
at 90 km	3 % in density	10 K in temperature

2. Due to the optic and electronic problems mentioned above, a source of systematic errors may appear in the measurements and is very difficult to evaluate. In order to estimate these errors, temperature profiles obtained

simultaneously at the two lidar sites during 65 nights have been compared. The two lidars are at the same latitude and 550 km apart; it is to be expected that the mean temperature profile will not be very different within this distance. At all altitudes between 30 and 80 km this difference has been found to be less than 2 K and this value is therefore an estimate of a possible systematic error. Comparison with radiosondes data at 30 km also indicate the same order of accuracy.

Data base

The data base consists of one mean temperature profile per night of measurement for each lidar site from October 1978 at OHP and March 1986 at BIS until the end of 1989 at both sites. The number of nights of measurements per month for each site is presented in Figure 1. During the recent years a mean value of eight nights per month is obtained at each site with a maximum as high as 19 nights per month in January 1984 at OHP. For the whole period the number of nights is 872 at OHP and 328 at BIS.

The two stations are located at the same latitude (44° N) from 550 km apart which is a short distance compared to the wavelengths of planetary waves (a few thousands of kilometers). It is then reasonable to consider that the climatology of the temperature is the same at the two sites and to use together all the data obtained at BIS and at OHP in a single set of data representative of the south of France. The number of profiles per month obtained this way allows a finer temporal description of the temperature variations.

Experimental Results

Mean Temperature

Data at OHP are of better quality and of extended height range since December 1983; the mean climatology of the temperature has been established by using data only from 1984 to 1989. Data obtained before 1984 will be used only to study long-term variations of the temperature.

The seasonal evolution of the temperature is obtained as follows: for each year from 1984 to 1989, data are interpolated to obtain one value per day and per kilometer. Data are smoothed with a 30-days FWHM Hanning filter. Finally for each day of the year the mean value is computed for the 6-year period and the results are presented in Plate 1 and tabulated in Table 2 by steps of 3 km in altitude and for the fifteenth of each month.

In spring and summer the evolution of the temperature is classical with the maximum at the stratopause and the minimum at the mesopause occurring in May/June, slightly before the summer solstice. In the upper stratosphere the minimum occurs at the beginning of November, one month and a half before the winter solstice, and is associated with a maximum in the 60- to 70-km range. A relative maximum is observed at the end of February in the middle stratosphere. The winter evolution may be explained by the frequent occurrence of upper stratospheric warmings in January and February, which increases the mean temperature during that period. A semiannual variation is seen clearly around 65 km with maxima in March/April and October/November.

The lidar climatology has been compared to the CIRA 1986 in which the contribution of planetary waves 1 and 2 has been included (Plate 2 and Table 3). Below 65 km the agreement between the lidar climatology and the CIRA 1986 is in general very satisfactory with differences smaller than 5 K, if we except a positive deviation observed in the middle stratosphere in February, corresponding to the frequent occurrence of stratospheric warmings during this month. In the altitude range of 65-80 km, lidar temperatures are in general colder than CIRA 1986 with a deviation larger than 10 K at 75 km in May and in November. On the contrary, positive deviations from CIRA 1986 are observed above 83 km with values as high as

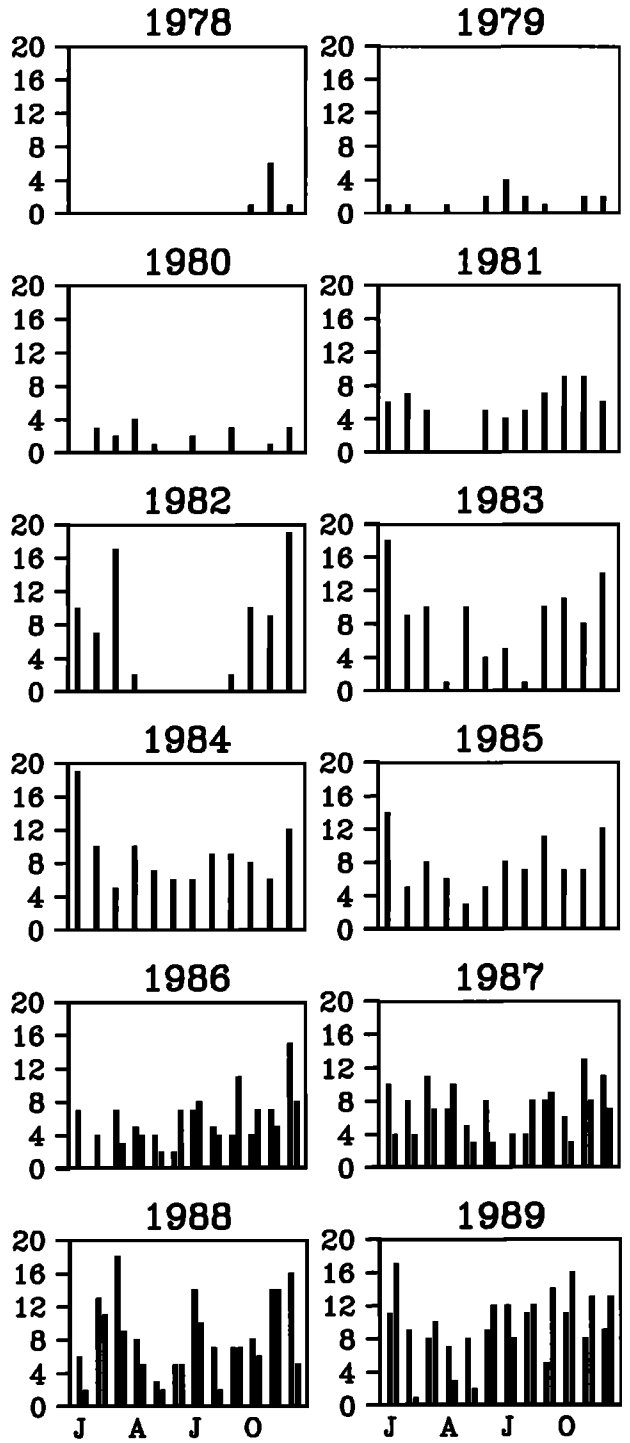

Fig. 1. Monthly number of data nights at OHP (solid) and BIS (shaded).

18 K at 87 km in September. Temperature profiles obtained at 45°N from SME limb scattering data [Clancy and Rusch, 1989], which are in good agreement with our lidar data in absolute value (see also Aikin et al. [1991] for the SME-lidar comparison), also show positive deviations compared to CIRA 1986 from 65 to 80 km and negative deviations above 80 km.

The mean temperature and its annual and semiannual components have been extracted by use of a least squares fit on data from 1984 to 1989 as explained in Appendix 1, but

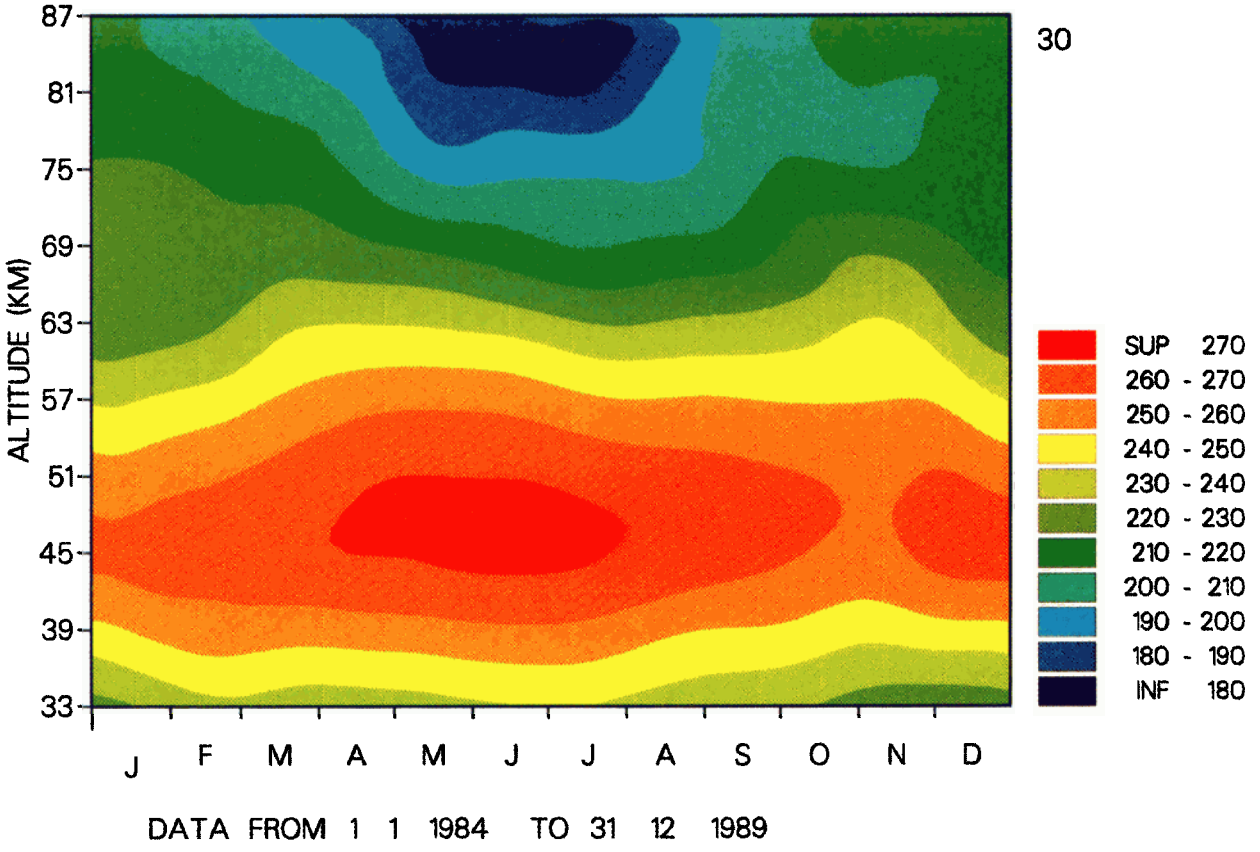

Plate 1. Time-height section of the temperature over the south of France obtained with data from 1984 to 1989. A 30-day Hanning filter has been applied to the data.

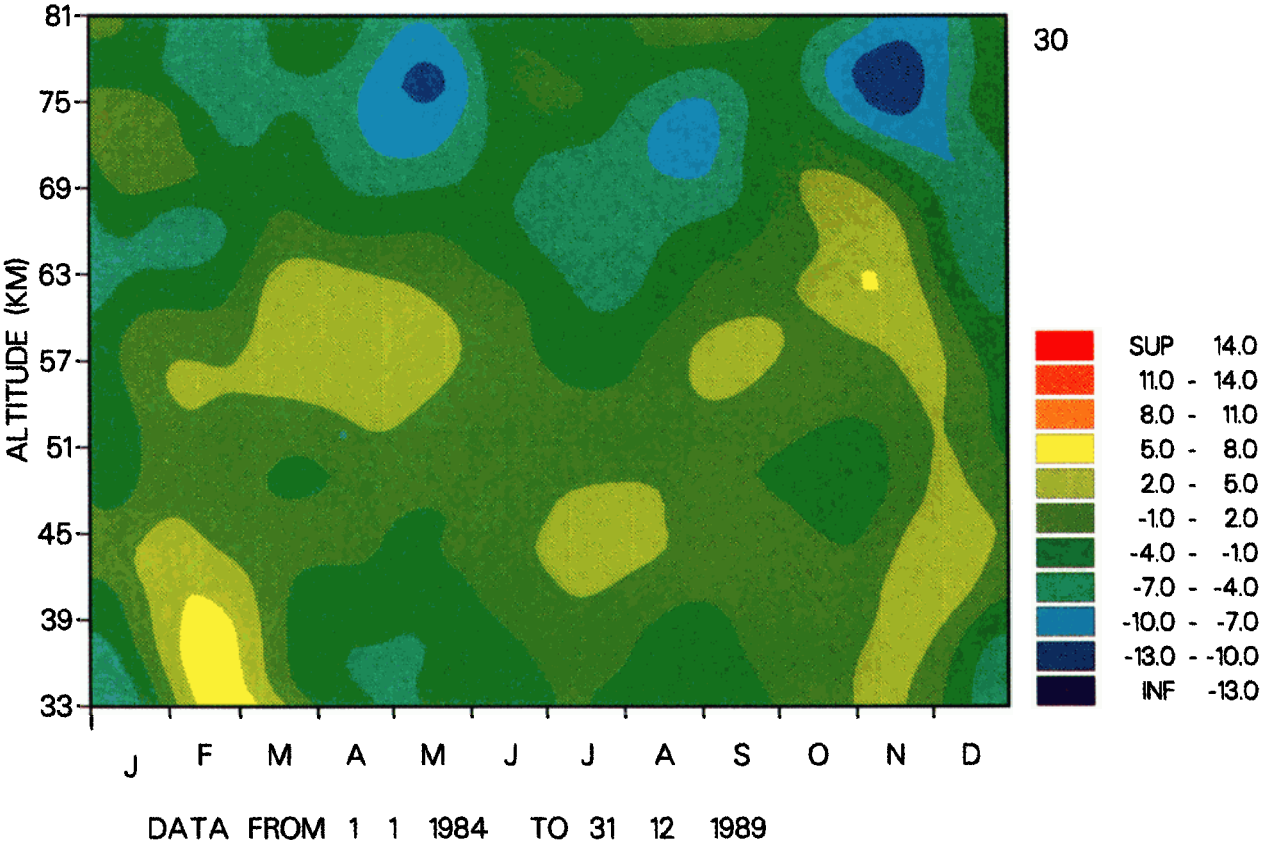

Plate 2. As in Plate 1 but for the deviation from CIRA 1986.

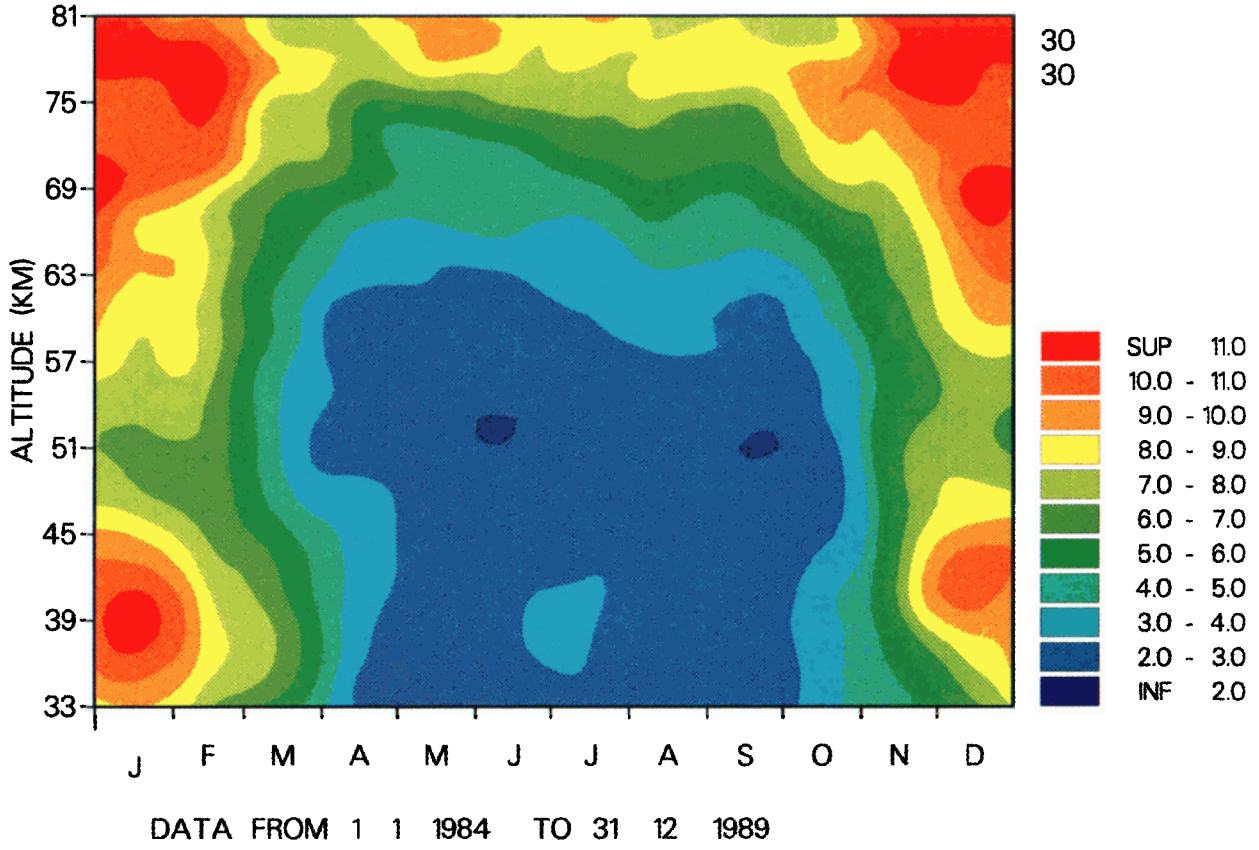

Plate 3. Standard deviation of the temperature (data from 1984 to 1989) corresponding to perturbations with 2-to 30-day periods (see text). A 30-day Hanning filter has been applied to the data.

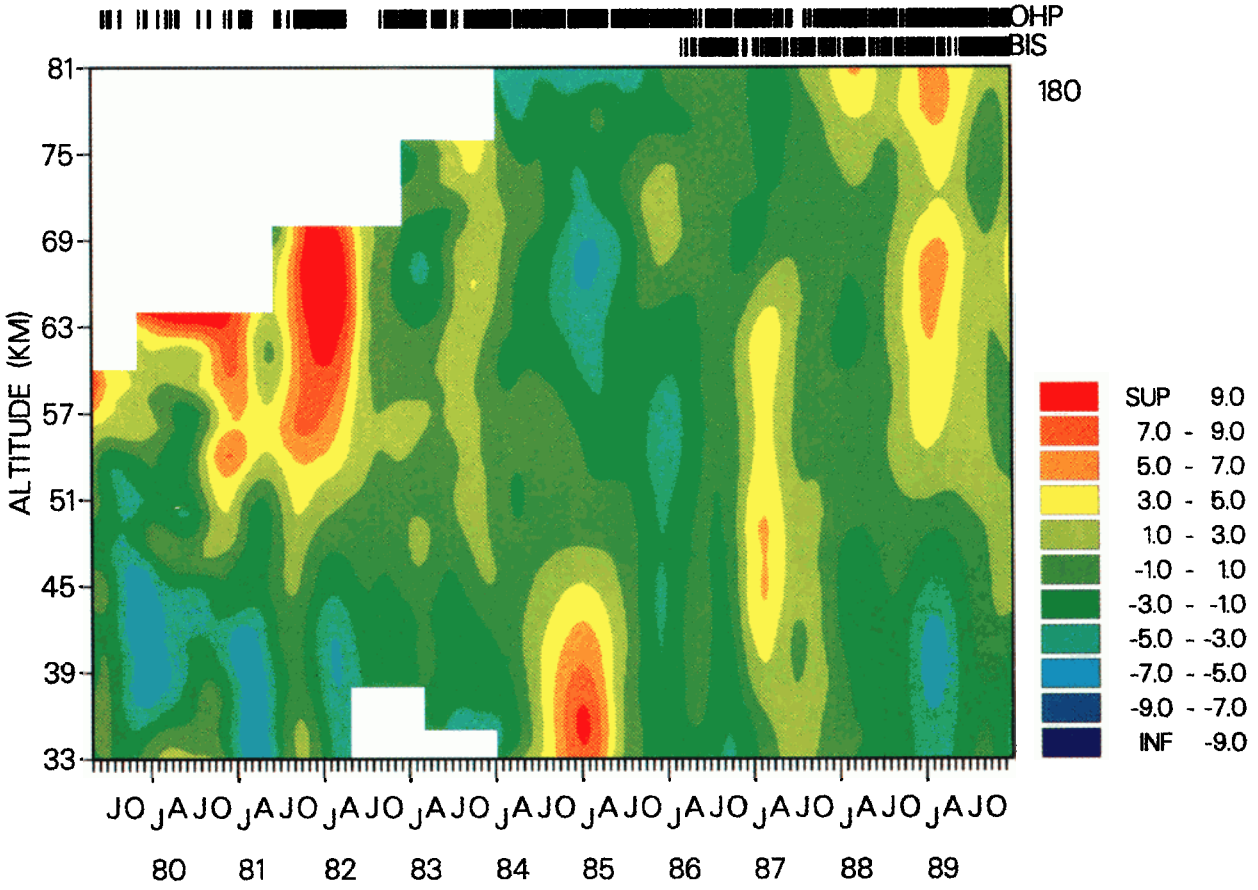

Plate 4. Temperature deviation from the climatological average presented in Plate 1. Dates of measurement at OHP and BIS are shown in the upper part of the figure. A 180-day Hanning filter has been applied to the data.

Table 2. Mean Temperature Profile Tabulated for the Fifteenth of Each Month (Data From 1984 to 1989)

Kilometer	Jan.	Feb.	March	April	May	June	July	Aug.	Sept.	Oct.	Nov.	Dec.
33	229.2	237.0	237.3	235.2	236.6	239.6	240.4	235.7	232.6	229.9	225.4	225.3
36	239.7	247.0	245.2	244.9	246.6	248.9	248.8	243.9	241.0	237.9	234.3	235.1
39	250.0	255.2	254.7	255.3	256.7	258.7	257.9	252.5	249.6	246.5	244.1	247.4
42	258.5	260.9	262.5	264.5	265.8	267.3	266.2	261.6	258.0	254.3	253.3	258.2
45	262.2	263.0	266.6	270.1	271.1	272.4	271.3	267.2	263.3	259.4	258.7	263.4
48	259.8	262.0	266.1	270.6	272.1	273.0	271.2	268.0	264.5	261.4	260.1	263.6
51	254.2	258.7	262.8	268.0	270.0	269.6	267.2	264.2	262.2	259.7	258.6	259.3
54	246.8	251.9	257.4	262.9	265.0	264.4	260.5	258.0	257.1	255.2	254.9	252.4
57	238.9	243.7	250.5	256.2	257.6	256.4	251.4	250.0	250.1	249.1	249.8	244.4
60	230.6	234.8	243.1	247.9	248.4	246.8	241.2	240.4	241.2	242.5	245.2	235.8
63	223.7	227.9	236.8	239.5	238.6	235.4	230.0	230.2	232.0	236.1	240.1	228.1
66	221.4	222.9	230.0	230.2	228.8	223.8	218.8	220.6	222.8	229.1	234.2	223.0
69	222.6	223.8	224.9	222.1	218.0	213.8	209.4	211.7	214.5	225.0	227.1	219.1
72	223.6	221.7	220.4	215.0	206.9	205.2	203.5	203.8	209.2	218.3	217.8	217.7
75	221.7	217.8	215.8	208.7	196.8	198.0	198.5	198.9	205.2	211.2	210.1	217.3
78	217.2	214.5	211.8	204.0	188.8	190.1	188.9	196.3	204.3	207.6	207.7	214.9
81	217.1	211.1	206.7	198.1	183.5	181.2	179.4	192.8	203.9	207.1	208.7	213.3
84	213.9	204.8	200.6	194.2	178.5	175.7	176.9	187.2	203.9	209.4	215.7	212.7
87	212.4	201.9	197.2	187.7	172.7	178.5	181.1	192.2	204.1	209.8	215.5	215.0

Table 3. Mean Temperature Deviation from the CIRA 1986 Tabulated for the Fifteenth of Each Month (data from 1984 to 1989)

Kilometer	Jan.	Feb.	March	April	May	June	July	Aug.	Sept.	Oct.	Nov.	Dec.
33	-5.9	5.8	3.5	-3.4	-3.9	-2.4	-0.9	-3.1	-2.4	0.6	2.5	-3.7
36	-3.5	6.7	0.7	-4.1	-3.9	-1.8	-0.1	-2.1	-1.3	0.9	2.7	-3.0
39	-1.2	5.8	0.3	-3.2	-3.2	-0.6	1.3	-1.1	-0.6	0.9	2.8	-0.1
42	0.8	4.1	0.2	-1.5	-1.9	0.4	2.6	1.1	0.5	0.5	2.5	2.9
45	0.7	1.8	-0.2	-0.3	-1.3	0.7	3.2	2.2	0.5	-0.9	1.0	3.1
48	-1.	0.4	-1.1	-0.2	-0.7	0.4	2.1	2.0	-0.3	-1.8	-0.6	2.2
51	-2.4	1.4	-0.4	0.9	0.4	-0.3	0.6	1.0	0.1	-1.3	-0.6	1.2
54	-1.6	2.0	1.6	2.8	1.9	0.2	-0.4	0.9	1.6	-0.1	0.6	0.7
57	-0.6	1.9	3.3	4.8	3.3	0.4	-2.0	0.3	2.9	1.2	1.9	0.1
60	-1.9	-0.5	3.3	4.5	2.9	0.2	-3.4	-1.5	1.9	1.8	3.8	-2.0
63	-4.2	-3.3	2.3	2.4	1.1	-1.4	-4.8	-3.3	0.2	2.4	4.3	-4.7
66	-3.6	-5.4	-0.5	-1.4	-1.1	-3.2	-6.0	-4.8	-2.2	1.7	3.2	-6.0
69	-0.4	-2.0	-2.2	-4.1	-4.1	-3.6	-6.4	-6.4	-4.7	2.7	0.1	-6.7
72	1.6	-2.4	-3.6	-5.9	-7.6	-3.2	-3.9	-7.6	-5.2	-0.1	-6.0	-6.0
75	0.5	-4.4	-4.5	-6.5	-10.1	-2.0	-0.9	-5.9	-5.1	-4.2	-11.1	-4.5
78	-2.7	-4.9	-3.9	-4.5	-9.8	-1.4	-2.3	-1.8	-2.2	-5.2	-11.4	-5.1
81	-0.9	-4.8	-3.6	-3.1	-6.8	-1.9	-3.7	1.5	2.0	-2.4	-7.8	-4.6
84	-0.5	-5.6	-2.6	1.3	-3.3	0.6	1.3	3.5	9.2	5.8	4.6	-1.5
87	4.5	-0.5	3.2	4.1	-1.2	9.8	11.5	16.4	18.6	14.8	12.8	7.8

without taking into account the long-term trend and the response to solar activity that will be discussed later. In the mean temperature profile (Figure 2) the stratopause is located at 47 km with a temperature of 267 K and the mesopause at 86 km with 196 K. The temperature gradient is maximum between 35 and 40 km with +3.2 K/km and minimum between 55 and 65 km with -2.7 K/km .

The annual wave (Figure 3) has a nearly constant amplitude of about 6 K from 33 to 57 km, a node at 65 km and an increasing amplitude up to the mesopause (21 K at 86 km). The maximum is observed in May-June, in phase with the solar heating below the node at 65 km and is in anti-phase with the solar heating above 65 km with a maximum occurring between November and January.

The semiannual wave (Figure 3) presents a maximum of amplitude of 6 K at 61-66 km, around the altitude of the node of the annual wave, which explains the quasi-purely semi-annual variation of the temperature at 65 km already mentioned.

Short-Term Variability Temperature

Previous climatologies of the temperature in the middle atmosphere did not take into account the notion of variance, which is very important when one has to use this climatology to forecast expected temperatures and to compare it with observed profiles. To study this variance we define a short-term variability V(t) as the standard deviation of the

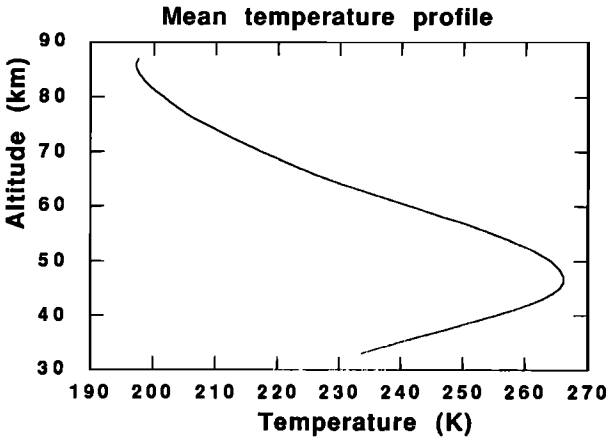

Fig. 2. Mean temperature profile over the south of France (data from 1984 to 1989).

temperature due to perturbations with periods ranging from 2 to 30 days. It is defined as a function of the temperature T(t) as

$$V(t)=\left[\overline{(T(t)-\overline{T})^2}\right]^{1/2}$$

In this formula the overbar denotes a Hanning filtering over 30 days. This variability is mainly due to the propagation of planetary waves. Data are integrated for 3 to 13 hours each night and then the contribution of the gravity waves tends to be eliminated, although long-period inertio-gravity waves may still contribute to the variability. Data are usually obtained during the first half of the night and then the contribution of tides, which become important above 65 km [Gille et al.,1991], may be neglected in this study.

In the stratosphere (Plate 3 and Table 4) the variability is maximum in December/January with values up to 10 K at 40 km and is lower than 3K from April to October. This variability is clearly related to the propagation of planetary waves and the occurrence of upper stratospheric warming during the period of strong westerly winds in the lower stratosphere in winter and the blocking of these waves when the wind blows from the east in spring and summer [Hauchecorne and Chanin, 1983].

In the mesosphere a minimum of variability is observed in winter just above the stratopause at 50-55 km, corresponding to a quiet layer between the upper stratospheric warmings and the associated mesospheric coolings, which leads to an important variability up to the higher levels. The minimum of variability from April to October still exists in the lower mesosphere up to 65 K, but above this level the variability remains large during the whole year (higher than 7 K at 78 km). The summer variability may be partly explained by the propagation of short-period planetary waves (for instance 2-day and 5-day waves) which are able to propagate through the easterly winds due to their high westward phase speed [Salby, 1984]. But another important phenomenon that more likely explains this variability is the occurrence of mesospheric temperature inversions due to the breaking of gravity waves above 70 km. Hauchecorne et al. [1987] have shown that these inversions even though more frequent in winter also appear in summer and may persist for several days. They should then contribute to the day to day variability all year round.

Long-Term Variability and Trend

As the lidar data base covers now a full 11-year solar cycle, the data have been analyzed in order to separate an eventual long-term trend of anthropogenic origin from the variation due to the 11-year cycle.

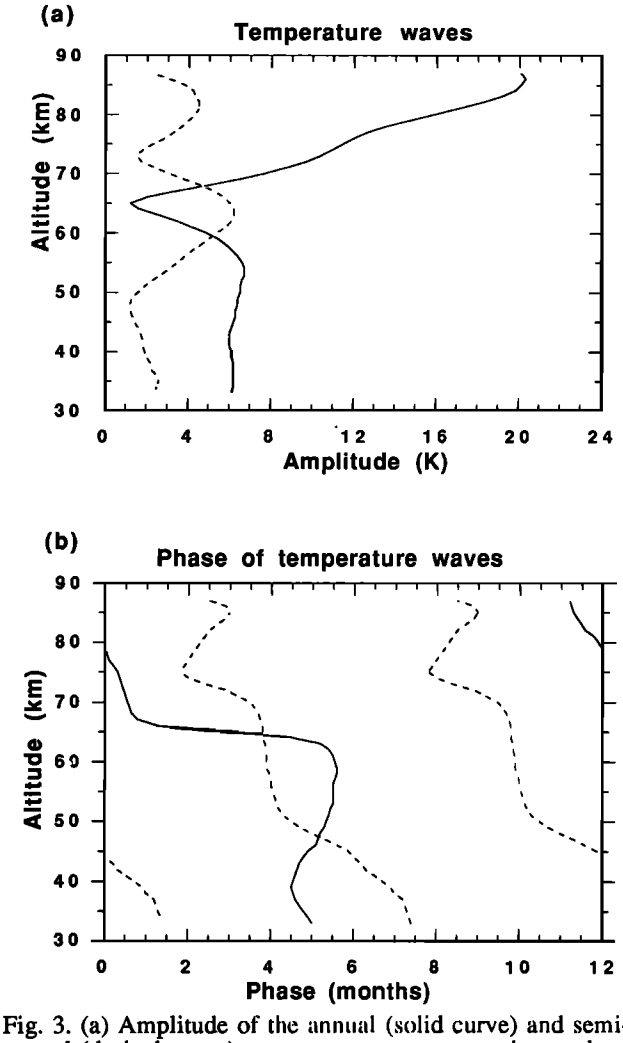

Fig. 3. (a) Amplitude of the annual (solid curve) and semi-annual (dashed curve) temperature waves over the south of France (data from 1984 to 1989). (b) Phase of the annual and semiannual temperature waves. A value of 0 for the phase corresponds to a maximum at the beginning of January and 12 at the end of December.

Data have been filtered with a 180-day Hanning filter to eliminate short-term variations due to planetary waves. The results between May 1979 and December 1989 are presented in Plate 4. The temperature presents quasi-periodic variations with 2 to 3 years periods probably associated with the QBO. A longer period evolution is also visible with cold temperatures in the stratosphere during the two solar maxima in 1979-1982 and in 1988-1989 and warm temperatures during the solar minimum in 1985-1987. In the mesosphere the temperature follows the opposite evolution with warm temperatures during the solar maxima and cold temperatures during the solar minimum.

In order to separate the response to the solar forcing from a long-term linear trend, a least squares fit has been made on data obtained from January 1979 to December 1989 using the method explained in Appendix 1 with an estimation of the confidence intervals as explained by Frederick [1984]. This fit has been first applied to the whole set of data with the seven parameters of the fit and second to the data obtained during the six "summer" months from April to September and the six "winter" months from October to March, but without the semi-

Table 4. Mean Standard Deviation of the Temperature Tabulated for the Fifteenth of Each Month (Data from 1984 to 1989)

Kilometer	Jan.	Feb.	March	April	May	June	July	Aug.	Sept.	Oct.	Nov.	Dec.
33	9.0	7.2	5.5	2.9	2.3	2.2	2.1	2.2	2.4	3.5	4.5	6.8
36	10.7	8.4	6.8	3.2	2.5	2.7	3.0	2.4	2.4	3.5	5.3	8.1
39	11.5	8.5	6.8	3.4	2.4	2.8	3.1	2.3	2.6	3.6	6.4	9.6
42	10.5	7.7	6.0	3.7	2.6	2.6	3.0	2.2	2.2	3.4	6.9	10.8
45	9.0	6.9	5.4	3.6	2.5	2.2	2.6	2.1	2.2	2.8	6.5	9.4
48	7.2	6.6	4.4	3.3	2.5	2.3	2.4	2.2	2.3	2.6	6.4	8.2
51	6.8	6.7	4.1	2.6	2.4	2.0	2.2	2.5	2.0	2.5	6.6	7.4
54	7.3	6.9	4.0	2.8	2.4	2.1	2.3	2.7	2.4	2.9	6.0	7.2
57	7.9	7.5	4.3	2.7	2.7	2.4	2.7	2.9	2.7	3.1	5.9	7.8
60	8.3	7.6	4.8	2.4	2.7	2.4	3.0	3.6	2.7	3.9	6.5	8.9
63	9.1	8.0	5.1	3.4	3.0	3.0	3.3	3.9	3.6	4.4	7.2	9.6
66	9.1	7.9	5.6	3.9	3.8	4.1	3.8	4.8	4.3	5.6	7.5	10.6
69	10.7	8.9	6.3	5.4	4.5	4.7	4.7	5.7	5.2	7.3	8.2	11.5
72	10.3	10.7	7.5	5.8	4.6	5.0	6.5	6.5	6.2	8.5	9.3	10.4
75	10.1	11.4	7.7	6.2	6.3	7.2	7.3	7.8	7.1	9.7	10.3	10.9
78	12.1	11.4	8.9	7.7	9.1	8.2	8.2	8.4	8.8	8.9	11.3	11.4
81	11.5	9.9	7.5	8.2	9.2	8.7	9.1	7.4	7.9	7.5	11.6	11.2

annual component, which is difficult to separate from the annual component with only six months of data per year.

The square root of the variance, obtained from the random term of the fit (see Appendix 1) (Figure 4a), is different from the short-term variability presented in Plate 3. It contains both the variability due to perturbations of periods longer than 7 days but shorter than 6 months and the interannual variability not taken into account by the fit. However, the results are quite similar to those presented in Plate 3, with values higher in winter than in summer and a relative minimum of variability near 50 km and large values all year round in the upper mesosphere.

The correlation between two successive 7-day profiles (Figure 4b) is nearly constant at 0.4-0.45 up to 65 km and decreases abruptly beyond 65 km to reach values lower than 0.2 at 75 km. These values correspond to a time constant t of the temperature autocorrelation (see Appendix 1) of about 9 days below 65 km decreasing to 4 days at 75 km. This result indicates that the variability is controlled by the planetary wave activity up to 65 km, with typical periods ranging from 1 week to 1 month, and by the breaking of gravity waves above 65 km which induces temperature perturbations as mesospheric inversions persisting a few days [Hauchecorne et al., 1987; Hauchecorne and Maillard, 1990].

When we consider the whole set of data (Figure 5a), the response to solar flux is well above the 95% confidence level and near the 99.99% level (about 4 σ) at maxima, with a negative response in the stratosphere and a positive response in the mesosphere. The maxima are obtained around 38 and 67 km with -3.8 K and +4.4 K/100 units of 10.7 cm flux (100 FU), respectively and a node is observed around 50 km. If this response is due to a radiative forcing of the middle atmosphere, we may expect a larger response in summer than in winter. The opposite is observed (Figure 5b for summer and Figure 5c for winter). The response has the same shape in summer as in winter but with a smaller amplitude. In summer the +2.7 K/100 FU response in the mesosphere is still significant at 95% due to a small confidence interval related to the low short-term variability of the atmosphere, but the -1.1 K/100 FU response in the stratosphere is well below the 95% level. In winter the -5.7 K/100 FU stratospheric and +5.4 K/100 FU mesospheric responses are significant at 95%, in spite of the large short-term variability. This difference in the

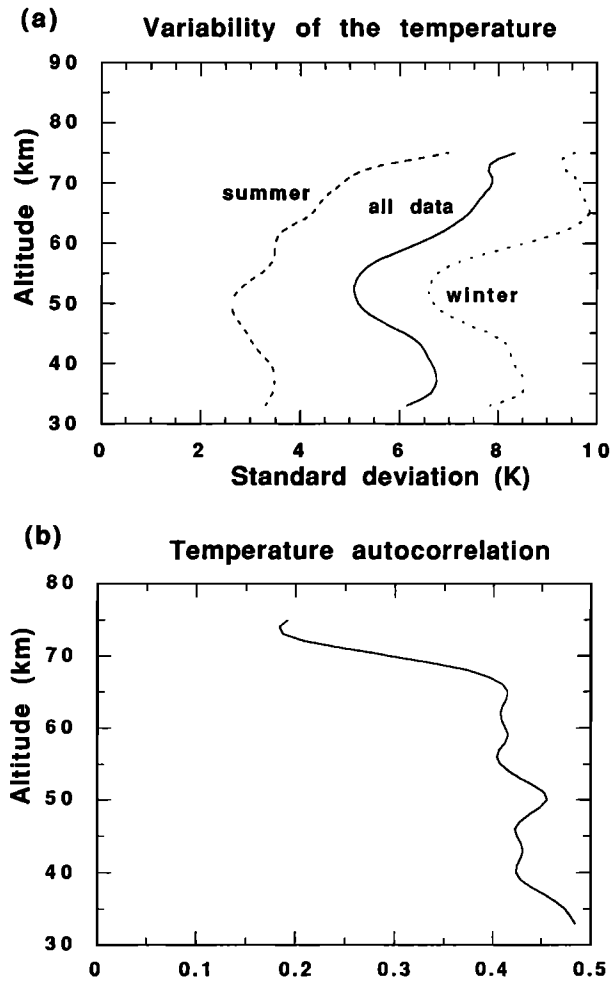

Fig. 4. (a) Variability of the temperature corresponding to the random term of the least squares fit (see Appendix 1). (b) Correlation between two successive 7-day mean temperature profiles.

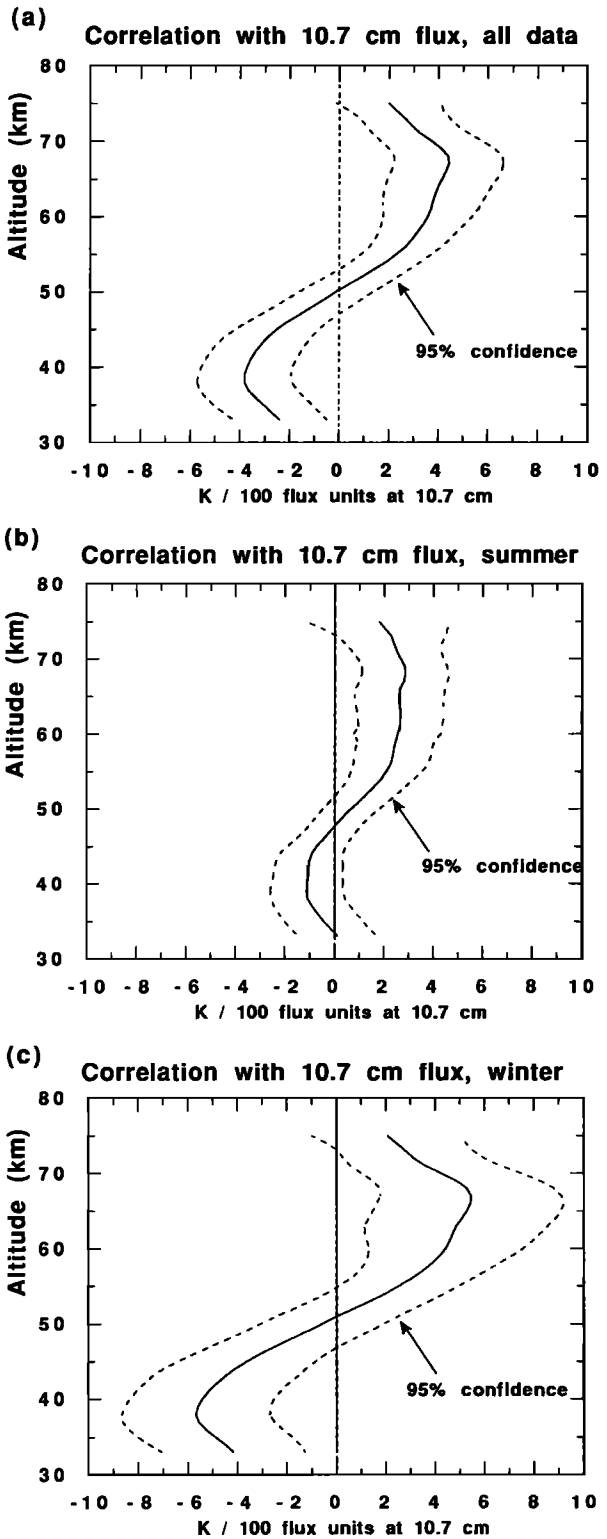

Fig. 5. Response to the 10.7-cm solar flux obtained with the least squares fit for (a) all the data , (b) summer months and (c) winter months (data from 1979 to 1989).

seasonal behavior indicates that we need to consider the role of the dynamics and in particular of the propagation of planetary waves in the possible link between the solar activity and the temperature of the middle atmosphere. The present study shows that a periodicity around 11 years exists in the lidar data. However, our data set covers only one solar cycle and one should be careful before concluding that this periodicity is due to the 11-year solar cycle and is not a natural fluctuation of the Earth atmosphere.

The linear trend observed on the whole set of data (Figure 6a) is positive but well below the 95% level in the stratosphere and negative in the mesosphere and at the limit of the 95%

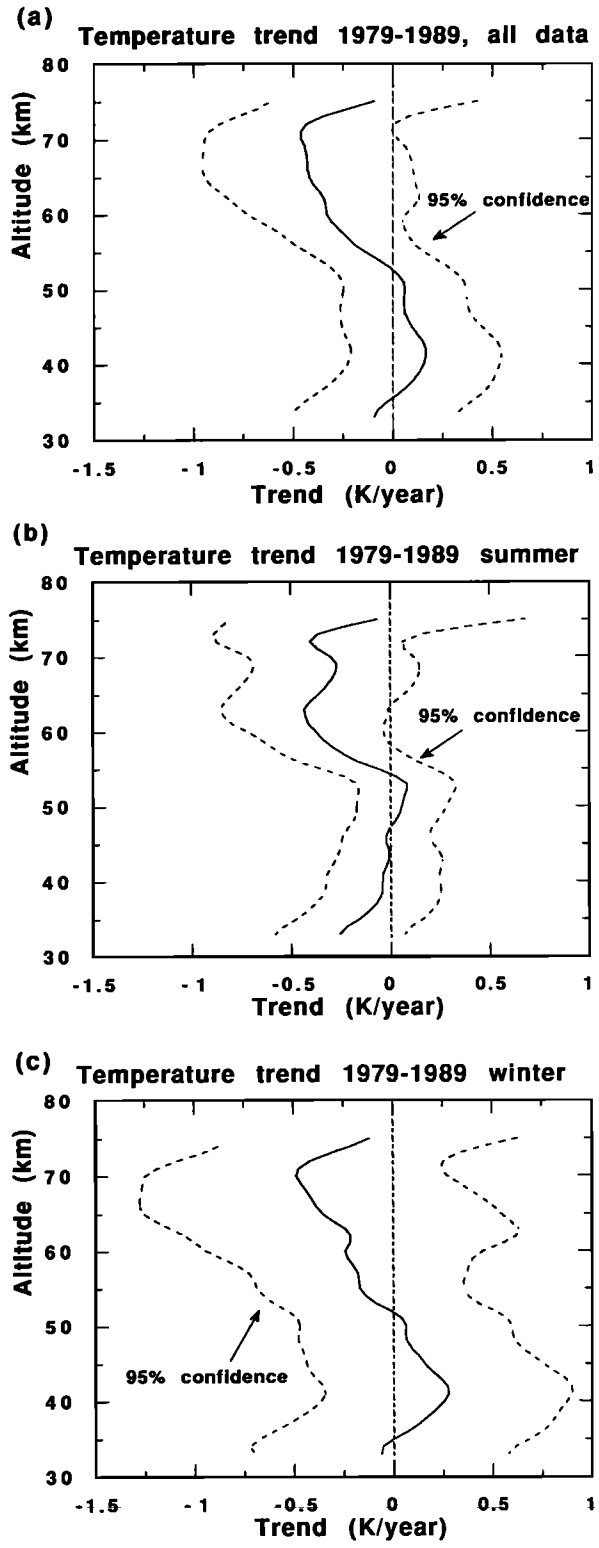

Fig. 6. As in Figure 5 but for the linear temperature trend.

level at 70 km with -4.6 K/decade. Due to the confidence interval being smaller in summer than in winter, we may expect an easier detection of the trend in the former case. This is true in the mesosphere where the negative trend is in the order of -4 K/decade between 60 and 70 km during both seasons (Figure 6b for summer and Figure 6c for winter) but above the 95% level in summer and not significant at all in winter. In the stratosphere no significant trend is observed in both seasons.

For the determination of a trend the confidence interval decreases rapidly when the number of observations n increases (it is proportional to $n^{-3/2}$ following Frederick [1984]). Furthermore the maximum of the present solar cycle occurred at the beginning of 1990. Data obtained during the decrease of the solar cycle will be crucial to confirm or to contradict the present results. For instance from our results in the mesosphere we expect a strong cooling near 65 km due to the positive response to the solar flux and the negative linear trend.

Discussion

In order to compare these results on long-term variability with previous observations, one has to be aware that trends have sometimes been deduced from data sets of very short duration (about half of a solar cycle). Since model predictions generally underestimate the amplitude of the solar influence, the incorrect estimate of the part due to the solar change led to large uncertainty on the determination of the trend itself.

Influence of the 11-Year Solar Cycle

The middle atmosphere between 30 and 70 km is expected to respond to changes in UV solar flux, in particular, the 11-year cycle period. The photo-chemical models [Garcia et al., 1984 ; Brasseur, 1989] predict a maximum effect of the 11-year solar forcing of +1 K at 50 km and a negligible effect out of the 30-to 70-km height range. This response is quite smaller than what was shown by observations and the disagreement stays unexplained.

Using radiosonde data, Labitzke and van Loon [1988] have shown that the temperature in the winter stratosphere at 30 hPa is correlated with the solar flux and that this correlation is improved when the data are separated according to the phase of the QBO. These results have been extended to the upper stratosphere and the mesosphere by Labitzke and Chanin [1988] using rocketsonde and lidar data and by Chanin et al. [1989] in the lower thermosphere. Keckhut and Chanin [1989] and Chanin [1989] have shown from lidar data at OHP from 1979 to 1988 that the observed effect for all seasons and independently of the sign of the QBO is -3 K/100 FU at 40 km and +7 K/100 FU at 65 km and that the correlation tends to become negative above 80 km. This last point is confirmed by the recent data of Neumann [1990] who found a negative response of -4K/100 FU at 86 km using OH temperature data obtained at Wuppertal (50°N, 7°E). A strong positive correlation between mesospheric temperature and solar flux is also observed at other sites of both high and low latitudes from rocketsondes data [Mohanakumar, 1989].

These results are also consistent with the cooling of the mesosphere during the descent of solar cycle n° 21 as observed by SSU (Channel 47X) between 1979 and 1986 [WMO, 1989] and SME temperature between 1982 and 1986 [Clancy and Rusch, 1989] which indicate changes of -1K/year at 0.5 hPa (about 55 km) and -1.5 K/year between 60 and 70 km respectively (the analysis of the lidar data during the period 1982-1986 indicates a negative trend of -1 K, -1.2 K, -1.7 K and -1.4 K/year at 55, 60, 65 and 70 km, respectively).

The whole set of observations gives the following picture: a positive response of 1 K below 30 km, a negative one of -3 to -4 K at 40 km turning to positive around 50 km with a maximum of +5 to +7 K between 60 and 70 km and again changing to negative at the mesopause height. Those results are confirmed by the results presented earlier but are not yet understood.

Anthropogenic trends

Global climatic models predict a warming of the troposphere due to the industrial emissions of carbon dioxide and other greenhouse gases such as CH_4, N_2O, CFCs [Hansen et al., 1983]. This warming should be associated with a cooling in the middle atmosphere, due to the IR emissions of these gases into space. Additional processes are likely to affect the stratosphere, among which are the ozone change and the increase in aerosol concentration. As a consequence of the induced radiative perturbations, dynamical processes and wave propagation could appear.

Therefore modelling of these complex interactions are not yet complete. The one-dimensional coupled photochemical model of Brühl and Crutzen [1988] for the scenario 1, the closest to the period 1960-1985, leads to a cooling of -1.5 K/decade for the recent past at 45-50 km. The two-dimensional model of Brasseur and Hitchman [1988] predicts a cooling of 20 K at 50 km for a doubling of CO_2 and an increase of Cl_x from 2.0 to 6.6 parts per billion in volume and its extention to the mesosphere by Roble and Dickinson [1989] predicts a 10 K cooling in the upper mesosphere for a doubling of CO_2 and CH_4. Using the 3-D Goddard Institute for Space Studies model which only includes the effect of greenhouse gases but takes into account changes in dynamics, Rind et al. [1990] obtained a lowest value of 10 K at 55 km. Within a factor of 2 the agreement between those recent models is quite satisfactory: they all indicate a maximum effect around 50 km and a rate of cooling between 1 and 2 K/decade for the present period. It is to be noted that these results are not very different from the results of earlier predictions by a dozen of 1-D radiative photochemical models which had been compared [WMO, 1989] and which predicted a cooling of -1.5 K to -1.7 K/decade in the 40- to 50-km layer.

The experimental evidence of trends suffers from the shortness of the data set. The longest series is clearly the one provided by radiosondes. Using the Berlin data set, Labitzke et al. [1986] found a negative trend in the temperature at 30 hPa from 1966 to 1980 of -0.24 K/decade over the whole northern hemisphere and -0.48 K/decade at 40°N. However in a recent publication van Loon and Labitzke [1990] raised the question of the significance of these results considering the high variability and the large amplitude of the 10-12 year oscillation. They concluded that more cycles of data were needed to detect an unambiguous trend. Above 30 km, data are of shorter extent if we except the rocket data for which the change of the calibration procedure in the early 1970s may be a source of uncertainty. However, using data obtained after the change, Angell [1987] found a linear trend for the period 1973-1985 of -0.4 K, -1.2 K and -2 K/decade in the 26-35, 36-45 and 46-55 km layers, respectively.

In the mesosphere, temperature data are fewer and cover one solar cycle at most. Recently, the SSU 47X data were reanalyzed and led to a temperature decline of 3.5 ± 0.5 K in the 1980-1990 decade at 0.5 hPa [Aikin et al., 1991]. Indirect evidence of a cooling has been observed by Taubenheim et al. [1990] from the reflection height of radio waves that showed a decrease of 10% of the air pressure at 80 km from 1962 to 1987 corresponding to an average 4 K cooling of the whole mesosphere (1.6 K/decade). Another indirect evidence can be provided by the occurrence of noctilucent clouds as suggested by Thomas et al. [1989]; Gadsen [1990] using a 25-year analysis of visual observations reports a 250% increase in noctilucent clouds occurrence which could be resulting from a cooling of 6.4 K over the same period of 2 K/decade at 90 km. As a summary, the trend observed by lidar in the mesosphere

is in good agreement with SSU channel 47X and compatible with the indirect evidence in the 80-90 km height range but 2 to 4 times larger than expected by the models.

On the contrary, the expected cooling of the stratosphere is not observed and even the lidar data seem to indicate a tendency toward a warming. This fact may be due to a change in the planetary wave activity during the period of analysis that tends to cancel the trend in the stratosphere and to amplify it in the mesosphere at the lidar site longitude. We have to keep in mind that our measurements are local and that models usually give zonal mean predictions. They may differ from local results as climatic conditions may generate cooling in some places and warming in others.

Conclusion

Data obtained by two Rayleigh lidars set up at OHP and BIS from 1978 to 1989 allowed us to obtain a unique set of data of 1200 nightly mean temperature profiles from 30 to 90 km. A climatology of the temperature in the middle atmosphere over the south of France has been established from this data base. The main results of this study are summarized below:

1. The observed temperature is in general colder than in the CIRA 1986 near 75 km and warmer above 80 km.
2. A clear semiannual variation is observed near 65 km with maxima occurring just after the equinoxes.
3. Below 65 km the short-term variability (periods ranging from 2 to 30 days) is maximum in December-January and very low from April to September. It is mainly due to the upward propagation of planetary waves with periods longer than 1 week.
4. Above 65 km a large short-term variability is observed during the whole year, associated with the breaking of gravity waves that induce temperature perturbations as mesospheric inversions persisting a few days.
5. A correlation with the solar flux, negative in the stratosphere and positive in the mesosphere, is found well above the 95% level. The response of the atmosphere is much larger in winter than in summer, which indicates the role of the dynamics in a possible link between the solar activity and the middle atmosphere. However with data covering only one solar cycle, it is very difficult to conclude that this link exists.
6. A cooling of the mesosphere of about -4 K/decade at 60-70 km is found but at the limit of the 95% confidence level, whereas no significant trend is observed in the stratosphere. Data obtained during the descent of the present solar cycle will be crucial to verify the existence of this long-term trend. These results on long-term variability are supported by direct or indirect results obtained from other sources.

Appendix 1: Least Squares Fit of the Data and Determination of the Confidence Intervals

A multiparameter least squares fit of the data has been applied to extract the different components included in the temporal evolution of the temperature at a given altitude (mean temperature, annual and semiannual variation, linear trend and response to the solar forcing). For this purpose each month is divided into four time intervals of 7-8 days, and a mean temperature profile is computed for each time interval for which at least one lidar profile is available. In the recent years lidar data are available during almost all periods and the temporal coverage is very good. The number of selected mean profiles is 378 from 1979 to 1989 (72% of the total) and 268 from 1984 to 1989 (93% of the total).

The temperature $T(z_i,t_j)$ at altitude z_i and time t_j (in years) is represented by

$$T(z_i,t_j)=\overline{T(z_i)}+A_1(z_i)\cos|(2\Pi t_j-\varphi_1(z_i))|+A_2(z_i)\cos|4\Pi(t_j-\varphi_2(z_i))|$$
$$+B(z_i)(t_j-\bar{t})+C(z_i)\left[\frac{F(t_j)-\bar{F}}{100}\right]+T'(z_i,t_j)$$

where

$\bar{t}$	mean value of t_j;
$\overline{T(z_i)}$	mean temperature at altitude z_i;
A_1, A_2	amplitude of annual and semiannual temperature waves;
φ_1, φ_2	phase of annual and semiannual waves (time of the maximum in year);
$B(z_i)$	linear trend of the temperature in K/year;
$C(z_i)$	solar flux component in K/100 units of 10.7 cm flux;
$F(t_j)$	10.7 cm solar flux at time t_j;
$\bar{F}$	mean solar flux during the period of analysis, $\bar{F}$=143.4 for 1979-1989;
$T'(z_i,t_j)$	random component of the temperature.

The method described by Frederick [1984] is used to determine the confidence interval for each parameter of the fit and in particular for the linear trend and the solar component. This confidence interval depends both upon the variance of the random component, which includes the short-term variability of the atmosphere and the measurement noise, and upon the correlation between two successive measurements. The variance of the temperature is defined as

$$\sigma^2_T(z_i)=\frac{1}{n-p}\Sigma_{j=1}^{n}T'^2(z_i,t_j)$$

where n is the number of profiles and p the number of parameters in the fit (p=7 when all parameters are taken into account).

The correlation between two successive measurements is

$$\phi(z_i)=\frac{\Sigma_{j=1}^{n-1}(T'(z_i,t_j)T'(z_i,t_{j+1}))}{\Sigma_{j=1}^{n-1}(T'^2(z_i,t_j)/2+T'^2(z_i,t_{j+1}))/2}$$

If we assume that the autocorrelation function decreases exponentially with a time constant t

$$\phi(t,t+\Delta t)=\exp(-\tau/\Delta t)$$

the least squares estimator for the linear trend is given by

$$\sigma^2(B(z_i))=\frac{(1-\phi^2(z_i))}{(1-\phi(z_i))^2}\frac{\sigma^2(T(z_i))}{\Sigma_{j=1}^{n}(t_j-\bar{t})^2}$$

and for the solar flux component by:

$$\sigma^2(C(z_i))=\frac{(1-\phi^2(z_i))}{(1-\phi(z_i))^2}\frac{\sigma^2(T(z_i))}{\Sigma_{j=1}^{n}\left(\frac{F(t_j)-\bar{F}}{100}\right)^2}$$

The 95% confidence interval is given by

$$\delta(B(z_i))=1.96\,\sigma(B(z_i)) \text{ and } \delta(C(z_i))=1.96\,\sigma(C(z_i))$$

Appendix 2: Linear Trend for the Period 1979-1990 in Summer

As mentioned earlier, the confidence interval in the detection of the long term trend increases quite rapidly with the

number of data. As an example, the linear trend obtained in summer including 1990 data is presented in Figure A1. It confirms the results presented in Figure 6b for the 1979-1989 period, but the negative trend observed in the mesosphere is now significant at the 95% confidence level in the interval 57-72 km.

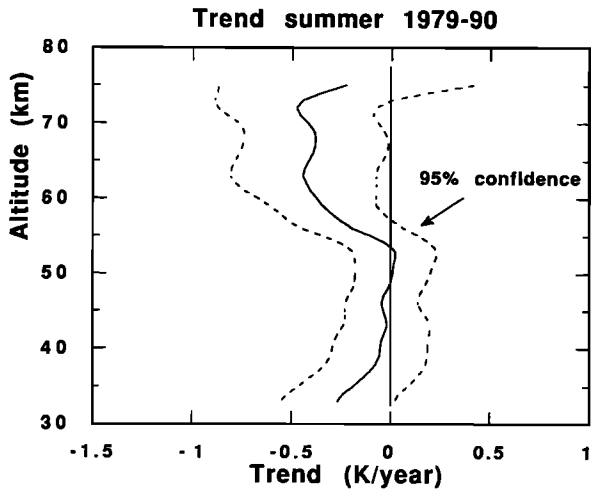

Fig. A1. Linear trend of the lidar temperature during summer months (data from 1979 to 1990).

References

Aikin, A. C., M. L. Chanin, J. Nash and D. J. Kendig, Temperature trends in the lower mesosphere, Geophys. Res. Lett., 18, 416-419, 1991.

Angell, J.K., Rocketsonde evidence for a stratospheric temperature decrease in the western hemisphere during 1973-1985, Mon. Weather Rev., 115, 2569-2577, 1987.

Barnett, J. J., and M. Corney, Middle atmosphere reference model derived from satellite data, Handbook for Middle Atmosphere Program, 16, 47-137, 1985.

Brasseur, G., The response of the middle atmosphere to change in solar activity, in Our changing atmosphere, 1989, 28th Liège International Astrophysical Colloquium, 255-264, Université de Liège, Cointe-Ougree, 1989.

Brasseur, G. and M. T. Hitchman, Stratospheric response to trace gas perturbations: changes in ozone and temperature distributions, Science, 240, 634-637, 1988.

Brühl , C., and P. J. Crutzen, Scenarios of possible changes in atmospheric temperatures and ozone concentrations due to man's activities, estimated with a one-dimensional coupled photochemical climate model, Climate Dynamics, 2, 173-203, 1988.

Chanin M. L, A review of the 11 year solar cycle, the QBO and the atmosphere relationship., Handbook for Middle Atmosphere Program, 29, 1989.

Chanin, M. L., and A. Hauchecorne, Lidar studies of temperature and density using Rayleigh scattering, Handbook for Middle Atmosphere Program, 13, 87-99, 1984.

Chanin, M. L., P. Keckhut, A. Hauchecorne and K. Labitzke, The solar activity-QBO effect in the lower thermosphere, Ann. Geophys., 7, 463-470, 1989.

Clancy, R. T. and D. W. Rusch, Climatology and trends of mesospheric (58-90 km) temperatures based upon 1982-1986 SME limb scattering profiles, J. Geophys. Res., 94, 3377-3393, 1989.

Curtis, P. D., J. T. Houghton, G. D. Peskett and C. D. Rodgers, The pressure modulator radiometer for Nimbus F, Proc. R. Soc. London, Ser. A, 337, 135-150, 1974.

Drummond, J. R., J. T. Houghton, G. D. Peskett, C. D. Rodgers, M. J. Wale, J. Whitney and E. J. Williamson, The stratospheric and mesospheric sounder on Nimbus 7, Philos. Trans. R. Soc. London, Ser. A, 296, 219-241, 1980.

Ellis, P., G. Holah, J. T. Houghton, T. S. Jones, G. Peckham, G. D. Peskett, D. R. Pick, C. D. Rodgers, H. Roscoe, R. Sandwell, Remote sounding of atmospheric from satellites. IV: The selective chopper radiometer for Nimbus 5, Proc. R. Soc. London, Ser. A, 334, 149-170, 1973.

Frederick, J. E., Measurement requirements for the detection of ozone trends, Ozone correlative measurements workshop, NASA Conf. Publ., 2362, B1-B19, 1984.

Gadsen, M., A secular change in noctilucent cloud occurrence, J. Atmos. Terr. Phys., 52, 247-251, 1990.

Garcia, R., S. Solomon, R. G. Roble and D. W. Rusch, Numerical response of the middle atmosphere to the 11-year solar cycle, Planet. Space Sci., 32, 411-423, 1984.

Gille, J. C., J. M. Russell III, P. L. Bailey, L. L. Gordley, E. E. Remsberg, J. H. Lienesch, V. W. G. Planet, F. B. House, L. V. Lyjak and S. A. Beck, Validation of temperature retrievals obtained by the Lilb Infrared Monitor of the Stratosphere (LIMS) experiment on NIMBUS 7, J. Geophys. Res., 89, 5147-5160, 1984.

Gille S.T., A. Hauchecorne and M. L. Chanin, Semidiurnal and diurnal effects in the middle atmosphere as seen by lidar, J. Geophys. Res., 96, 7579-7587, 1991.

Hansen J., G. Russell, D. Rind, P. Stone, A. Lacis, A. Lebedeff, R. Ruedy and L. Travis, Efficient three-dimensional global models for climate studies: Models I and II, Mon. Weather Rev., 111, 609-662, 1983.

Hauchecorne, A. and M. L. Chanin, Density and temperature profiles obtained by lidar between 35 and 70 km, Geophys. Res. Lett., 7, 565-568, 1980.

Hauchecorne, A. and M. L. Chanin, Mid-latitude Lidar observations of planetary waves in the middle atmosphere during the winter of 1981-1982, J. Geophys. Res., 88, 3843-3849, 1983.

Hauchecorne, A., M. L. Chanin and R. Wilson, Mesospheric temperature inversion and gravity wave breaking, Geophys. Res. Letters, 14, 933-936, 1987.

Hauchecorne, A. and A. Maillard, A 2-D dynamical model of mesospheric temperature inversions in winter, Geophys. Res. Letters, 17, 2197-2200, 1990.

Keckhut, P.and M. L. Chanin, Seasonal variation of the 11 year solar effect on the middle atmosphere; role of the QBO, Handbook for Middle Atmosphere Program, 29, 33-38, 1989.

Labitzke, K. and M. L. Chanin, Changes in the middle atmosphere in winter related to the 11-year solar cycle, Ann. Geophys., 6, 643-644, 1988.

Labitzke, K., G. Brasseur, B. Naujokat and A. De Rudder, Long term temperature trends in the stratosphere: possible influence of anthropogenic gases, Geophys. Res. Letters, 13, 52-55, 1986.

Labitzke, K. and H. van Loon, Association between the 11-year solar cycle and the atmosphere. Part I: the troposphere and stratosphere on the northern hemisphere in winter, J. Atm. Terr. Phys., 50, 197-206, 1988.

Lefrère, J., J. Pelon, C. Cahen, A. Hauchecorne and P. Flamant, Survey of the post Mt. St. Helens stratospheric aerosol at Haute-Provence Observatory, Appl. Opt., 7, A70, 1981.

Miller, D. E., J. L. Brownscombe, G. P. Carruthers, D. R. Pick and K. H. Stewart, Operational temperature sounding of the stratosphere, Philos. Trans. R. Soc. London, Ser. A, 296, 65-71, 1980.

Mohanakumar, K., Influence of solar activity on middle atmosphere associated with phases of equatorial QBO, Handbook for Middle Atmosphere Program, 29, 39-42, 1989.

Neumann A., QBO and solar activity effects on temperatures in the mesopause region, J. Atmos. Terr. Phys., 52, 165-173, 1990.

Rind, D., R.Suozzo, N. K. Balachandran and M. J. Prather, Climate change and the middle atmosphere, J. Atmos. Sci., 47, 475-494, 1990., 1990.

Roble, R. G. and R. E. Dickinson, How will changes in carbon dioxide and methane modify the mean structure of the mesosphere and thermosphere? , Geophys. Res. Lett., 16, 1441-1444, 1989.

Salby, M. L., Survey of planetary scale traveling waves: the state of theory and observations, Rev. Geophys., 22, 209-236, 1984.

Schmidlin, F. J., Repeatability and measurement uncertainty of United States meteorological rocketsonde, J. Geophys. Res., 86, 9599-9603, 1981.

Taubenheim, J., G. von Cossart and G. Entzian, Evidence of CO2-induced progressive cooling of the middle atmosphere derived from radio-observations, Adv. Space Res., 10, 171-174, 1990.

Thomas, G. E., J. J. Olivero, E. J. Jensen, W. Schroeder O. B. Toon, Relation between increasing methane and the presence of ice clouds at the mesopause, Nature, 338, 490-492, 1989.

Van Loon, H. and K. Labitzke, Associating between the 11-year solar cycle and the atmosphere. Part IV: The stratosphere not grouped by the phase of the QBO, J. of Climate, 3, 827-837, 1990.

WMO (World Meteorological Organization), Trends in stratospheric temperatures, Global ozone research and monitoring project, Rep. 20, vol. 1, chap. 2.4; 235-244, Geneva, 1989.

M. L. Chanin, A. Hauchecorne, and P. Keckhut, Service d'Aéronomie du Centre National de la Recherche Scientifique, BP3, 91371 Verrières le Buisson, France.

(Received December 12, 1990;
revised March 15, 1991;
accepted March 19, 1991.)